



UV-light irradiation preparation of soybean residue-based hydrogel composite from inorganic/organic hybrids for degradable slow-release N-fertilizer

Chengyi Wu^{1,2} · Liping Wang¹ · Huiting Kang¹ · Youmeng Dan¹ · Dating Tian¹ · Yin Zheng¹

Received: 29 April 2019 / Accepted: 8 November 2019 / Published online: 18 November 2019
© Springer Nature B.V. 2019

Abstract

Biomass waste, which was the by-product generated along with the production of food, was transformed into high-value constituent in slow-release fertilizers. This approach could reduce the cost of fertilizer application and improve the degradation performance. In this study, a novel slow-release nitrogen fertilizers (SNFs) from inorganic/organic hybrids, based on soybean residue-g-poly(acrylic acid)/polyethylene glycol 2000/kaolin/urea, was prepared via UV-light radiation and characterized by Fourier transform infrared spectroscopy, X-ray diffraction, scanning electron microscopy and thermogravimetric analysis. The mechanical testing result demonstrated that the compressive modulus of the sample was 62.19 MPa. The water absorbency of SNFs was 51.2 g/g in distilled water. The swelling behavior of SNFs in pH, saline types and concentration solutions indicated its excellent pH and salt sensibility. The water-holding of soil was 72.3% with the SNFs of 3%. The release result of SNFs in soil was only 63.4% within 30 d. The release mechanism was coincident with non-Fickian diffusion.

Keywords Soybean residue · Kaolin · Inorganic/organic hybrids · Slow-release fertilizer

✉ Chengyi Wu
wcyfz@126.com

¹ Department of Chemistry and Environmental Engineering, Hubei Minzu University, Enshi 445000, Hubei, China

² Key Laboratory of Biologic Resources Protection and Utilization of Hubei Province, Enshi 445000, Hubei, China

Introduction

Chemical fertilizer is an important factor to boost grain production. N is used as plant nutrition with the greatest influence on the growth of plants. Among these N fertilizers, urea is the most widely used due to its high N content, low cost and ease of application [1, 2]. However, the traditional urea was dissolved so fast that it did not absorb completely by crop. A large amount of nutrient was discharged into the environment, which resulted in huge economic losses and environmental pollution, such as eutrophication of water body, soil acidification and groundwater pollution [3, 4]. Considering these issues, slow-release fertilizers attracted much more attention owing to their excellent property, which could improve fertilizer use efficiency [5–7].

At the same time, many farmlands are suffering from the shortage of water resources in the arid region. The application of superabsorbent polymers (SAPs) in the agriculture field could improve water-holding capacity of the soil, reduce irrigation frequency and lower death ratio of plants. Biomass-based SAPs have attracted much more attention due to their abundance, renewability, cost-effectiveness and biodegradability compared to petroleum-based SAPs [8]. Soybean residue (SBR) is a by-product generated during edible oil, *tofu* (Chinese) or soymilk production processes, which is produced in huge quantities annually in China. About 2,800,000 tons of SBR from the *tofu* industry every year was produced; furthermore, the consumption of SBR increases obviously in European countries [9]. In Asian countries, about 800,000 tons and 310,000 tons *tofu* were produced every year in Japan and Korea, respectively [10]. However, SBR was not abundantly used for high-value product except for primitive utilization for low-grade farmyard manure in many areas of the world. Therefore, it is necessary to improve the use value of SBR. SBR contains high content of dietary cellulose and hemicellulose, the functional groups of which are hydroxyl and amino groups [11]. These functional groups could graft with vinyl monomers and cross-linker to form SAPs. However, few studies have reported that SBR was used as a raw material to prepare SAPs. Introduction of low-cost SBR into SAP formulation not only improves its biodegradation, but also reduced proportion of the acrylate-based monomers in its composition. However, the application of SAPs was limited due to its high cost. In order to solve this problem, low-cost kaolin was introduced to polymer matrix in high proportions due to the reactive –OH groups on its surface, high specific surface area, swelling capacity and valuable cation exchange capacity. Meanwhile, the organic constituents present toughness, low density, good elasticity and formability [12]. Polyethylene glycol (PEG), a kind of nonionic hydrophilic polyether, displayed excellent environmental compatibility and was widely used as a drug carrier, water-holding and absorbent material. PEG was used to construct a semi-interpenetrated network to improve the surface and network structure, swelling capacity and slow-release properties [13].

With the increase in environmental protection, many new methods were used in chemical synthesis, such as microwave irradiation [14, 15], ultrasound [16], electron-beam irradiation [17–19], γ -irradiation [20] and UV-light irradiation

[21]. Among these methods, UV-light irradiation could shorten reaction time and improve reaction efficiency.

In this manuscript, we attempted to one-step prepare a SNF based on SBR, acrylic acid (AA), PEG2000, kaolin and urea via UV-light irradiation. The structures and morphology of samples were characterized using Fourier transform infrared spectroscopy (FT-IR), X-ray diffraction (XRD) and scanning electron microscopy (SEM). The swelling measurements in different environments, the largest water-holding ratio (WH%) and water retention capacity (WR%) of soil with SNFs and the release behavior of SNFs in soil were systematically investigated.

Experimental

Materials

Soybean residue (SBR, available from commercial sources) was washed and dried at 80 °C in an oven for 10 h and then pulverized to filtrate with 40 mesh; it mainly contains 51.4% dietary cellulose, 26.2% protein, 11.5% lipid and other constituents. 2,2-Dimethoxy-2-phenylacetophenone (DMPA) and *N*-methyl pyrrolidone (NMP) were obtained from Guangzhou Chemical Reagent Factory. Sodium hydroxide, hydrochloric acid, *N,N'*-methylenebisacrylamide (MBA) and urea were purchased from Guoyao Chemical Reagent Co. Ltd. Kaolin was taken from Fuchen Chemical Reagent Co. Ltd.; it was immersed in 0.1 mol/L HCl solution for 24 h and washed with distilled water into neutral before using. Acrylic acid (AA) was taken from Fuchen Chemical Reagent Co. Ltd; para-dimethylaminobenzaldehyde and polyethylene glycol 2000 (PEG2000) were purchased from Aladdin; other chemical reagents were all of analytical grade.

Preparation of SNFs

In this procedure, 4.0 g AA (neutralization degree 70%), 1.0 g PEG2000, 1.0 g urea and 0.5 g MBA were added into a 250-mL round-bottom flask containing 0.5 g SBR and 1.0 g kaolin previously dispersed in 50 mL of distilled water. DMPA (20wt %, relative to dried SBR), which was firstly dissolved in the NMP solution to form 2.5% w/w concentration, was added as a UV-initiating agent. Then, the flask was exposed under the ultraviolet light for 1 h. The self-installed UV irradiation apparatus consisted of an iron box containing a UV lamp (365 nm, 1000 W, Philips). The mixture was protected under the N₂ atmosphere in the whole process. The resulting gel products were immersed in 100 mL 70% (v/v) ethanol and changed every 24 h in order to remove uncross-linked polymer and unreacted reagents. Finally, the resulting products (SBR-g-PAA/PEG2000/kaolin/urea) were dried in an oven at 70 °C until a constant weight milled, sifted and marked as SNFs. A schematic illustration of the forming and release pathway of SNFs is presented in Fig. 1.

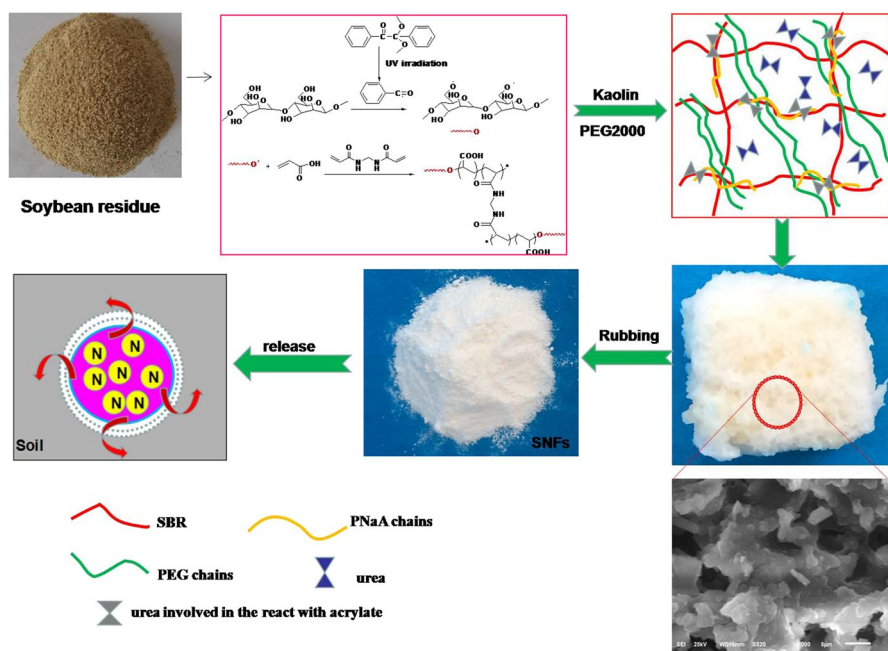


Fig. 1 Schematic illustration of the forming and release pathway of SNFs

Characterization

The structures of products were confirmed by Fourier transform infrared spectroscopy (FT-IR, model spectrum-2). The samples were subjected to wave numbers from 400 to 4000 cm^{-1} . Scanning electron microscopy (SEM, Hitachi X650) was used to investigate the surface morphology of samples. X-ray diffraction measurements were conducted using an X-ray diffractometer (XRD, 7000S/L, SHIMADZU). The XRD patterns were taken from 10° to 70° with a speed of $10^\circ/\text{min}$ to collect 2 θ data using CuK α radiation. The thermal stability of the samples was determined by the thermogravimetric analyzer (ATGA-Q500, TA Instruments, New Castle, USA). Each sample was performed in the temperature range of 20–600 $^\circ\text{C}$, heating rate of 5 $^\circ\text{C}/\text{min}$ and N_2 flow of 60 mL/min. Mechanical properties of samples with dimensions of 10 mm \times 10 mm \times 10 mm were conducted at 25 $^\circ\text{C}$ using a compression apparatus (Instron 3366, USA) at a constant crosshead speed of 2 mm/min. The compressive modulus was obtained from the initial (straight line) linear slope of the stress versus strain curve, and the results were the average of three measurements.

Swelling measurement

0.1 g sample was immersed, respectively, into 250 mL distilled water, different kinds and concentrations of saline solutions (NaCl , NH_4Cl , MgCl_2 , CaCl_2 , AlCl_3 , FeCl_3)

and different pH solutions until the swelling equilibrium was reached; the sample was taken out, the surface water of which was absorbed by a filter paper. The SR of the sample was calculated according to Eq. (1):

$$SR \text{ (g/g)} = \frac{W_2 - W_1}{W_1} \quad (1)$$

where W_1 is the weight of the dry sample (g) and W_2 is the weight of the swelled sample(g).

WH% and WR% of soil with SNFs

In order to study the effect of SBR-g-PAA/PEG2000/kaolin/urea on the water-holding capacity of the soil, the maximum water-holding capacities of soils with different ratios of hydrogel were determined based on the Liu's method [22]. 1, 2, 3 wt% (to dry soil) SBR-g-PAA/PEG2000/Kaolin/urea were mixed with 150 g dry soil (particle size less than 1 mm), respectively. And then, the mixture was put into a PVC pipe with a diameter of 4.5 cm. The bottom of the pipe was sealed with a non-woven cloth and weighed (signed W_1). The soil samples were irrigated with water from the top of the pipe until the water seeped out from the bottom. The tube was weighed again (signed W_2). All experiments were repeated in triplicate. The maximum water-holding of soil (WH%) is calculated by Eq. (2):

$$WH\% = \frac{(W_2 - W_1)}{150} \times 100\%. \quad (2)$$

The beaker was weighed at first (marked W_0). A certain weight of sample powder was well blended with 100 g dry soil (below 20 mesh), then the mixture was placed in a beaker, and then 25 g water was added slowly into the soil and the whole container was weighed (W_1). The beaker was kept at 25 °C in an air oven and weighed (marked W_i) at a certain time interval. The soil without sample powder was also conducted. The water retention (WR%) was calculated according to Eq. (3) [23]:

$$WR\% = \frac{W_i - W_0}{W_1 - W_0} \times 100\%. \quad (3)$$

Slow-release behavior

The release behavior of SNFs in water was studied according to Liu's method [24]. The dried samples were placed in non-woven cloth and immersed in 100 mL distilled water. At certain time intervals, 10 mL solution was taken out for the determination of urea solution. In order to maintain a certain amount of solvent, 10 mL distilled water was added into the beaker. The urea released from SNFs was dyed with para-dimethylaminobenzaldehyde, the concentrations of which were determined at 426 nm by UV-visible spectrophotometer.

In order to investigate the release behavior of SNFs in soil, an experimental procedure was conducted according to Olad's method [25]. 100 g of dry soil (below 25 mesh) was mixed with 1.5 g SNFs sample. The mixture is then placed into a 4.5-cm-diameter column with non-woven fabric and valves. Then, the water was added to the column until the water was adsorbed to a saturation state. During the whole process, the content of water in the column retained constantly. At a certain interval (every 24 h to 30 days), 10 mL solution was collected. The concentrations of urea in the solution were determined by UV–visible spectrophotometer. The release experiments were repeated in triplicate, and the average value was the final result.

In order to study the mechanism of release, the cumulative release data were evaluated by Pitger–Peppas as given in Eq. (4):

$$\frac{M_t}{M_\infty} = Kt^n, \quad (4)$$

where M_t/M_∞ is the percentage of nutrient release at different time t . K is the rate constant. n is the release index, which determines the release mechanism of the nutrient.

Degradation of SNFs

In order to imitate the field conditions of farmland, the degradation behavior of SNFs was investigated in soil solution. 100 g of soil was immersed in 500 mL distilled water for 24 h. The supernatant was obtained by centrifugation, and then, the pH of the solution was determined. Then, the SNFs have been cut into thin slices (7 mm in diameter, 1.5 mm in thickness) and placed into the soil solution at room temperature; the weight of SNFs was dried to constantly, and recorded after taking out from soil solution at 2, 4, 10, 15, 20, 30, 40, 50, 60th day. The degradation of SNFs is calculated according to Eq. (5):

$$\text{Degradation (\%)} = \frac{M_0 - M_i}{M_0} \times 100\% \quad (5)$$

where M_0 and M_i are the weight of un-degradation and degradation, respectively.

Results and discussion

Characterization

FT-IR spectra of SBR, urea, kaolin, PEG and SNFs are shown in Fig. 2. In Fig. 2a, the absorption peak at 3436 cm^{-1} was attributed to the stretching vibration of hydrogen-bonded OH. The peak at 2915 cm^{-1} was caused by methylene. The absorption peak was observed at 1754 cm^{-1} , which was due to the stretching vibration of C=O of amide I band. The band at 1430 cm^{-1} was assigned to the stretching vibration of carbonyl. The peak at 1120 cm^{-1} was caused by b-1,4-glycosidic bond, which was

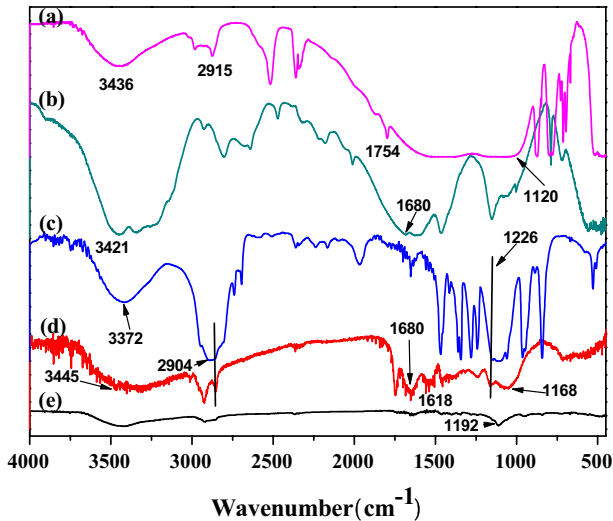


Fig. 2 FT-IR spectra of SBR (a), urea (b), PEG2000 (c), SNFs (d) and kaolin (e)

typical absorption peak of cellulose [26]. Figure 2b shows the FT-IR spectrum of urea; the characteristic peaks at 3445 and 1680 cm^{-1} were attributed to the stretching vibration of $-\text{NH}_2$ and $\text{C}=\text{O}$, which was also displayed in the spectrum of SNFs. In the spectrum of PEG2000 (Fig. 2c), the peaks at 3445 and 2904 cm^{-1} were also observed and ascribed to the stretching vibration of $-\text{OH}$ and $-\text{CH}_2$. The strong adsorption peak at 1226 cm^{-1} was due to the stretching vibration of $-\text{O}-$. In the spectrum of kaolin (as shown in Fig. 2e), the adsorption peak at 3452 cm^{-1} was attributed to the OH stretching mode of inner hydroxyl groups. The peaks observed at 1192 cm^{-1} were assigned to the stretching of $\text{Si}-\text{O}$. In the FT-IR spectrum of SBR-g-PAA/PEG2000/kaolin/urea (as shown in Fig. 2d), the adsorption peaks at 3445 and 1680 cm^{-1} were observed and caused by the stretching vibration of $-\text{NH}_2$ and $\text{C}=\text{O}$ in $-\text{CONH}_2$. This finding demonstrated the involvement of urea in SBR-g-PAA/PEG2000/kaolin/urea [27]. In addition, the new absorption peaks were found at 1618 and 1168 cm^{-1} , which were resulted from the stretching vibration of $\text{C}=\text{O}$ of acrylamide and the bending vibration of $\text{N}-\text{H}$. This information implied that acrylamides were formed by condensation reaction between urea and AA [11].

The XRD spectra of samples are shown in Fig. 3. A broad peak at $2\theta = 15.8^\circ$ was assigned to crystal structure of SBR (Fig. 3a). The characteristic peak of kaolin was reflected at $2\theta = 26^\circ$ (Fig. 3b). The characteristic peaks of PEG2000 were displayed at $2\theta = 19.1^\circ$ and 24.6° (Fig. 3c). The characteristic peaks at $2\theta = 23.6^\circ$, 24.5° , 32.4° were attributed to the crystal structure of urea (as shown in Fig. 3d). Meanwhile, the characteristic peaks of SBR, kaolin, PEG2000 and urea were reflected in XRD spectrum of SNFs (Fig. 3e), which indicated that the SNFs were prepared successfully.

Figure 4 displays the surface patterns of samples; the picture of SBR shows almost smooth and wrinkle surface with low porosity (as shown in Fig. 4a). However, Fig. 4b exhibits the surface morphology of SBR-g-PAA/urea, which has an

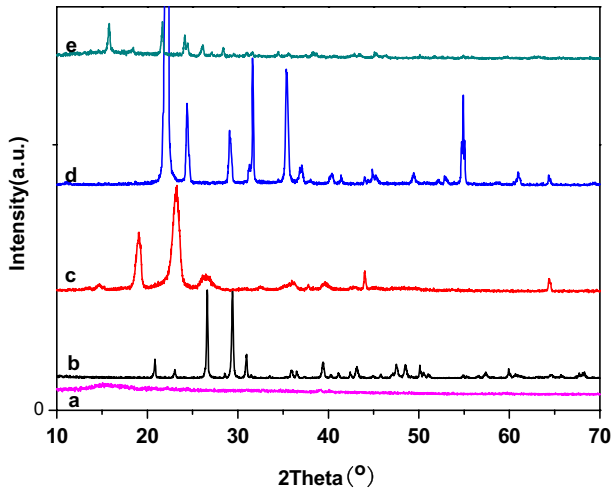


Fig. 3 XRD spectra of SBR (a), kaolin (b), PEG2000 (c), urea (d) and SNFs (e)

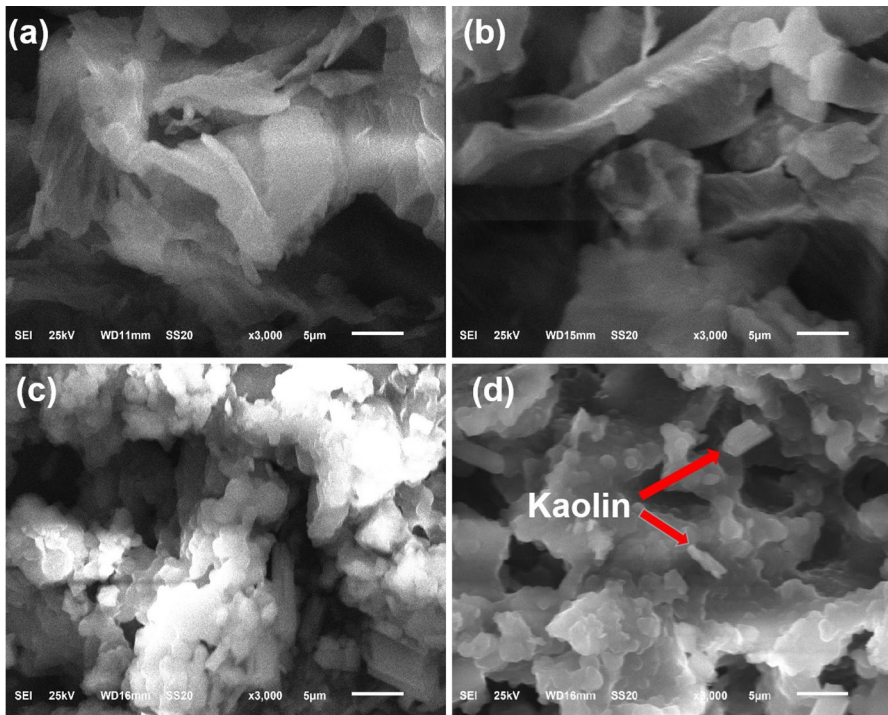


Fig. 4 SEM micrographs of SBR (a), SBR-g-PAA/urea (b), SBR-g-PAA/PEG2000 (c) and SNFs (d)

undulant and porous structure. These discrepancies between their surface structures were attributed to the formation of many irregular aggregates during the graft copolymerization reaction between SBR and AA. The surface morphology of SBR-g-PAA/PEG2000 is displayed in Fig. 4c; the number of pores and open channels increased in comparison with SBR-g-PAA, which revealed that the introduction of PEG influenced the surface morphology of samples. While the SEM of SNFs (Fig. 4d) also revealed that the linear PEG2000 chains effectively interpenetrated the composite network without flocculation, a homogeneous composite was formed. Moreover, kaolin particle was well dispersed in the polymer network. The above information indicated that the increase in surface area of samples was due to the introduction of PEG chain and kaolin, respectively.

The TG and DTG diagrams of SBR and SNFs are depicted in Fig. 5. The TG profiles of SBR exhibited two steps. The first step from room temperature to 150 °C with 5% weight loss was due to the evaporation of adsorbed water. The second step in the range of 160–550 °C with the weight loss of 65% was attributed to the decomposition of dietary cellulose and fat. Meanwhile, three peaks in DTG profiles at 65.12, 259.17 and 325.64 °C exhibited the maximum decomposition speeds. Differently, the TG curves of SNFs showed three steps. The first step from room temperature to 150 °C with about 5% mass loss was ascribed to the evaporation of water molecules. However, the maximum decomposition speed of water was improved to 133.29 °C, which was assigned to the interaction between H₂O and composite. The second stage occurred within 160–278 °C with 20% mass loss, which was caused by the disintegration of PEG2000 and cellulose. Specifically, it displayed the disintegration of branches or side chain groups of the graft copolymer. Finally, the third step was taken place in the range of 278–550 °C with the weight loss of 41%, which could be attributed to the decomposition of the main chain of the copolymer. It is observed in Fig. 5b that the maximum decomposition speed of 325.64 °C was improved to 407.62 °C, which was due to the incorporation of kaolin into the composite and the formation of polymeric network. The thermal stability of SNFs is better than that of SBR.

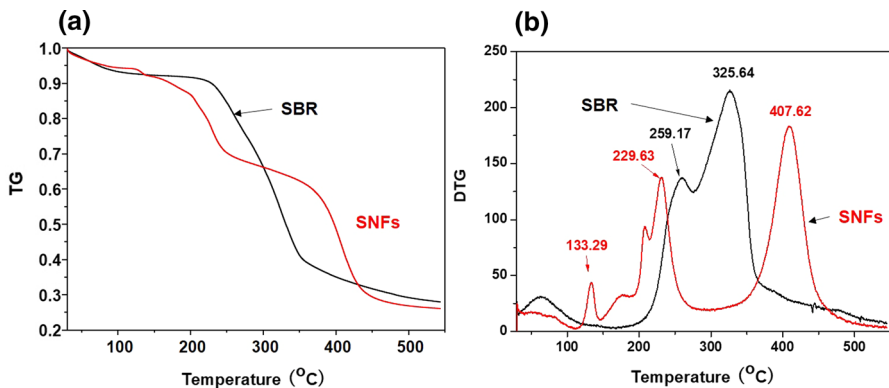


Fig. 5 TG (a) and DTG (b) thermograms of SBR and SNFs

Mechanical properties

Figure 6 shows the compressive stress–strain curves of SBR-g-PAA/urea and SNFs. It was clearly shown that the elastic region of SNFs was reduced in comparison with SBR-g-PAA/urea. Meanwhile, the compressive stress at fracture of SNFs was greater than that of SBR-g-PAA/urea. The compressive stress of SBR-g-PAA/urea was 2.31 MPa at 63.8% fracture strain, while that of SNFs increased to 11.4 MPa at 83.4% fracture strain. Moreover, the compressive modulus increased from 10.34 MPa for SBR-g-PAA/urea to 62.19 MPa for SNFs. The phenomenon was attributed that the addition of kaolin formed a dense and rigid network structure.

Swelling of SNFs

Figure 7a shows the swelling curve of SNFs in distilled water. Initially, the swelling ratio increased sharply and is then followed by a slower rate until the maximum swelling ratio (51.2 g/g) was reached at 12 h. This phenomenon could be attributed to kaolin, which acted as the physical cross-linking agent.

The SNF contains a large amount of $-\text{COO}^-$ and $-\text{COOH}$ groups, the protonation degree of which is mainly dependent on the change of pH value of medium. Therefore, the SR is intently related to the pH value of medium. The effects of different pH values on the SR of the sample are shown in Fig. 7b. The SR increased with the increase in pH in the range of 2–8 and then decreased when the pH increased from 8 to 12. The highest SR of the sample is 43.2 g/g. This finding was assigned to the transformation of $-\text{COO}^-$ to $-\text{COOH}$, and the formation of hydrogen bond among $-\text{COOH}$ under acidic conditions weakened the electrostatic repulsive force of $-\text{COO}^-$ and decreased the SR of the sample. Afterward, with pH increasing, partial $-\text{COOH}$ was ionized to $-\text{COO}^-$, which enlarged the anion–anion electrostatic repulsion and resulted in an increase in water invading

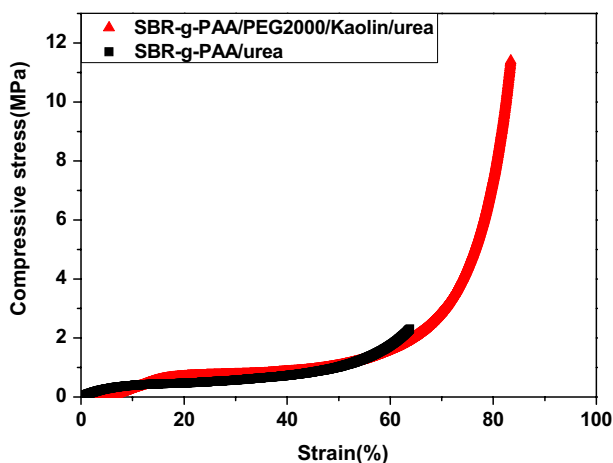


Fig. 6 Mechanical property testing of samples

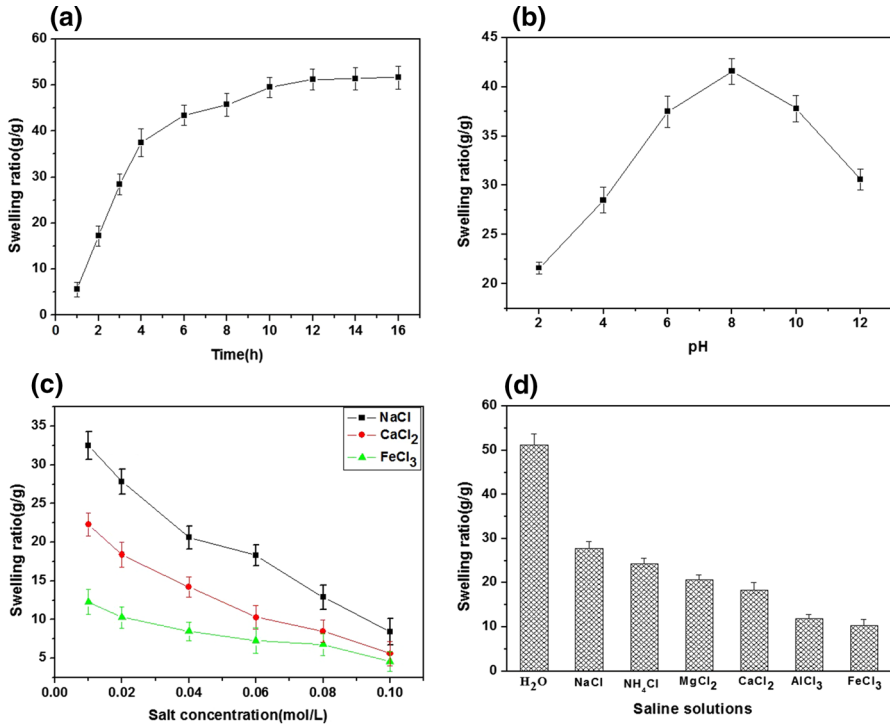


Fig. 7 Effects of time (a), pH (b) and saline concentrations (c) and types (0.02 mol/L) (d) on swelling ratio of the SNF sample

[28]. However, when the pH was further increased ($\text{pH} > 8$), the SR of the sample decreased. The fact was caused by the effect of charge shielding for excess Na^+ added from NaOH [29].

The effects of different saline concentrations and types on the SR of product are shown in Fig. 7c, d. From Fig. 7c, it is observed that the SR of the sample decreased with the increase in saline concentrations. This phenomenon was explained that the osmotic pressure decreased with the increase in saline solution concentration, which resulted in a decrease in water absorbency. Namely, as shown in Fig. 7d, the SR of SNFs in saline solutions was lower than that of value in distilled water. This phenomenon was explained by the charge screening effect of the cations. These cations could shield the $-\text{COO}^-$ and prevent the anion–anion repulsions, which results in a decrease in the osmotic pressure between hydrogel network and the external medium and a consequent reduction in the SR of product. Meanwhile, the SR order of the sample in 0.02 mol/L saline solutions was as follows: $\text{Na}^+ > \text{NH}_4^+ > \text{Mg}^{2+} > \text{Ca}^{2+} > \text{Al}^{3+} > \text{Fe}^{3+}$. This finding was mainly attributed to the formation of intra- or intermolecular complexes between multivalent cations and $-\text{COO}^-$ on SNFs, which weakened the electrostatic repulsion among carboxylate group, therefore inducing less water to penetrate into the internal

network of product [30]. Moreover, in saline solutions with multivalent cations, the SR of the sample decreased with the increase in cation charge from divalent (Mg^{2+} , Ca^{2+}) to trivalent (Al^{3+} , Fe^{3+}). This finding was due to the increase in cross-link density. Moreover, it was clearly displayed that the SR in monovalent cationic solutions (Na^+) was higher than that measured in polyatomic cationic solution (NH_4^+). Furthermore, the less the radius of the multivalent metal cation, the higher the SR ($\text{Mg}^{2+} > \text{Ca}^{2+}$ and $\text{Al}^{3+} > \text{Fe}^{3+}$).

Water-holding and water retention behavior of SNFs

The water-holding ratios of soil with different application rates of SNFs are shown in Fig. 8a. The largest water-holding ratios are 31.2, 54.2, 63.8 and 72.2% for SNF application ratios of 0, 1, 2 and 3%, respectively. It was clearly shown that the addition of SNFs to soil could improve the water-holding capacity of the soil. The water content increased with an increase in SNF content in the soil. Therefore, the soil which was mixed with these SNFs could retain much more water during the irrigation period or rain than the soil without it. These could efficiently reduce the consumption of irrigation water [31, 32].

Figure 8b demonstrates the water retention capacity of soil with different application rates of SNFs. It was clearly shown that the water retention capacity of soil improved with an increase in SNF content. After water retention measuring for 8 days, the water retention capacity of soil without SNFs had decreased to 0%. However, the water retention capacities of soil with different SNF rates of 1% and 2% decreased to 0% when the time prolonged to 18d and 28d, respectively. Therefore, it has been proven that the soil with the addition of SNFs could effectively reduce the consumption of agricultural irrigation water.

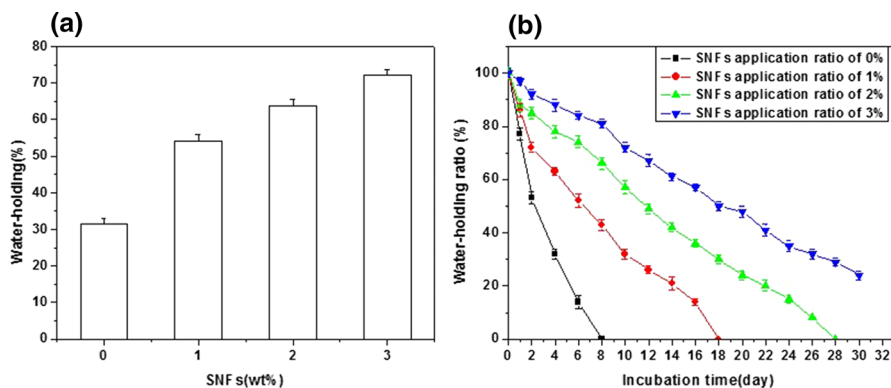


Fig. 8 Water-holding (a) and water retention (b) of soil with different application ratios of SNFs

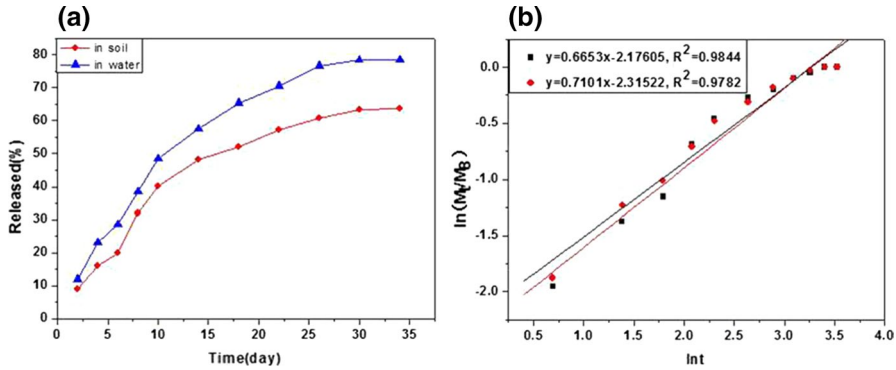


Fig. 9 Release behavior (a) and released kinetic (b) of SNFs in water and soil

Table 1 Release kinetic parameters of SNFs

	R^2	K	n
In water	0.9844	0.1135	0.6653
In soil	0.9782	0.0987	0.7101

Slow-release behavior of SNFs

Figure 9a shows the release profile of SNFs in water and soil. It was clearly shown that the release ratios of N in water and soil with 30d were 78.3% and 63.4%, respectively. This finding was attributed to several factors as follows: (1) The nutrient was difficult to diffuse out of the composite hydrogel, which resulted from SNFs which could be slowly swollen by the soil solution after it was added into soil [33]. (2) A tortuous path was generated after the addition of kaolin, which would complicate the path of N through the network [34]. (3) The adsorption and steric effects of SNFs took effect on the diffusion of nutrient after the SRFs being added into soil, which led to reduction in the release rate of nutrient [26].

In order to study the release mechanism of SNFs, Korsmeyer–Peppas model was employed to appraise the data. The correlation coefficient (R^2), rate constants (K) and release index (n) are listed in Table 1. The result demonstrated that the n values of SNFs in H₂O and soil were between 0.5 and 1, which indicated that the release mechanism of urea was non-Fickian diffusion or chain relaxation control release. This phenomenon indicated that the release behavior occurred due to the multiple mechanisms of diffusion and swelling-controlled release [35].

Degradability of SNFs

In recent years, with the increasing awareness of environmental protection, the problem that pure polyacrylate resin is difficult to degrade encourages people

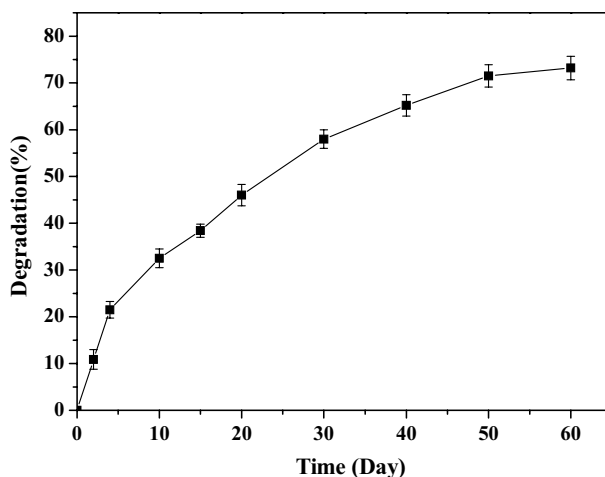


Fig. 10 Degradation of SNFs in the soil solution

to study biodegradable material with high water retention activity. In this work, Fig. 10 represents the degradation curve of SNFs at room temperature in the soil solution with $\text{pH}=7.5$. At the same time, the degradation degree increased with the time prolonging. The degradation degree of SNFs reached 72% after degradation in the soil solution for 60 days. The reason was that the chips of SNFs were immersed in the soil solution and swelled, and the water molecules diffused into the network of product. At the same time, the degradation occurred with the time prolonging; the cleavage of ether bond between $-\text{CH}_2\text{OH}$ and $-\text{OH}$ or two $-\text{CH}_2\text{OH}$ occurred in the process of degradation. The cross-linking density of network decreased with the ongoing break of cross-links increased. Then, the fact water molecules diffused into the network become more easily when the pore of network enlarged, which is similar to that reported in the literature [36, 37].

Conclusion

In summary, a novel SBR-based SNF with superadsorbent function was prepared via UV-light irradiation and characterized. FT-IR and XRD results displayed that PEG chains interpenetrated the polymer network and combined with the network. SEM and TG analysis confirmed that the addition of kaolin was conducive to the pore structure and thermal stability. It was clearly shown that the swelling behavior of SNFs was influenced by pH, saline types and concentrations. The study indicated that the water-holding and water retention of soil were improved obviously with the addition of SBR-g-PAA/PEG2000/kaolin/urea. The slow-release results of SNFs showed that the product had preferable slow-release property. The release kinetic studies of fertilizer confirmed that the developed SNF formulations follow a non-Fickian diffusion mechanism. Moreover, the degradation of SNFs in the soil solution was studied. Thus, the SNFs based on SBR were expected to be used widely in agriculture and horticulture fields.

Acknowledgements This work has been supported by the National Natural Science Foundation of China (No. 21767009); the Young Talents Project of Science and Technology Research Program of Education Department of Hubei (Q20171905); the Science Research Group of Hubei University for Nationalities (MY2014T007); the Doctoral Science Research Foundation of Hubei University for Nationalities (MY2013B017); the Open Science Foundation of Key Laboratory of Biological Resources Protection and Utilization of Hubei Province (PKLHB1912); and the Special Funds for “Double First-Class” Construction in Hubei Province.

References

1. S.G. Zhang, Y.C. Yang, B. Gao, Y.S. Wan, Y.C. Li, C.H. Zhao, J. Agric. Food Chem. **64**(28), 5692 (2016)
2. A. Schneider Teixeira, L. Deladino, N. Zaritzky, A.C.S. Sustain. Chem. Eng. **4**(4), 2449 (2016)
3. L. Zhou, D. Cai, L. He, N. Zhong, M. Yu, X. Zhang, Z. Wu, A.C.S. Sustain. Chem. Eng. **3**(4), 645 (2015)
4. C. Vudjung, S. Saengsuwan, J. Polym. Environ. **26**, 3967 (2018)
5. B.R. Araújo, L.P. Romão, M.E. Doumer, A.S. Mangrich, J. Environ. Manag. **190**, 122 (2017)
6. D. An, B. Liu, L. Yang, T.-J. Wang, C. Kan, Chem. Eng. J. **311**, 318 (2017)
7. X. Xiao, L. Yu, F. Xie, X. Bao, H. Liu, Z. Ji, L. Chen, Chem. Eng. J. **309**, 607 (2017)
8. P. Wen, Y.J. Han, Z.S. Wu, Y.H. He, B.-C. Ye, J. Wang, Arab. J. Chem. **10**(7), 922 (2017)
9. I. Mateos-Aparicio, C. Mateos-Peinado, P. Rupérez, Food Sci. Emerg. Technol. **11**, 445 (2010)
10. S.H. Ahn, S.C. Oh, I. Choi, G. Han, H. Jeong, K. Kim, Y. Yoon, I. Yang, J. Hazard. Mater. **178**, 604 (2010)
11. B. Li, M.Y. Qiao, F. Lu, Food Rev. Int. **28**, 231 (2012)
12. M. Likhitha, R. Sailaja, V. Priyambika, M. Ravibabu, Int. J. Biol. Macromol. **65**, 500 (2014)
13. Y.F. Chen, Y.H. Sun, Z.H. Yang, X.H. Lu, X.Y. Ji, Appl. Energy **257**, 113962 (2020)
14. H. Ge, W. Pang, D. Luo, Carbohydr. Polym. **66**, 372 (2006)
15. C.-X. Lin, H.-Y. Zhan, M.-H. Liu, S.-Y. Fu, L.-H. Huang, J. Appl. Polym. Sci. **118**, 399 (2010)
16. T. Wan, R. Huang, Q. Zhao, L. Xiong, L. Qin, X. Tan, G. Cai, J. Appl. Polym. Sci. **130**, 3404 (2013)
17. S. Zhang, W. Wang, H. Wang, W. Qi, L. Yue, Q. Ye, Carbohydr. Polym. **101**, 798 (2014)
18. K.M. El Salmawi, S.M. Ibrahim, Macromol. Res. **19**, 1029 (2011)
19. H.L.A. El-Mohdy, A. Safrany, Radiat. Phys. Chem. **77**, 273 (2008)
20. G.R. Bardajee, Z. Hooshyar, F. Zehtabi, A. Pourjavadi, Iran. Polym. J. **21**, 829 (2012)
21. X. Shi, W. Wang, A. Wang, J. Polym. Res. **18**, 1705 (2011)
22. L.H. Xie, M.Z. Liu, B.L. Ni, Y.F. Wang, J. Agric. Food Chem. **60**, 6921 (2012)
23. A. Li, J. Zhang, A. Wang, Bioresour. Technol. **98**, 327 (2007)
24. L.H. Xie, M.Z. Liu, B.L. Ni, Y.F. Wang, Ind. Eng. Chem. Res. **51**, 3855 (2012)
25. R. Azam, A. Oald, R. Adel, Polym. Bull. **72**, 2667 (2015)
26. X.D. Li, Q. Li, Y. Su, Q.Y. Yue, B.Y. Gao, Y. Su, J. Taiwan Inst. Chem. Eng. **55**, 170 (2015)
27. P. Wen, Z.S. Wu, Y.H. He, B.-C. Ye, Y.J. Han, J. Wang, X.Y. Guan, ACS Sustain. Chem. Eng. **4**(12), 6572 (2016)
28. H.L. Wei, H. Wang, H.J. Chu, J.J. Li, Int. J. Biol. Macromol. **133**, 1210 (2019)
29. A. Olad, H. Zebhi, D. Salari, A. Mirmohseni, A. Tabar, Mater. Sci. Eng. C **90**, 333 (2018)
30. T. Zhou, Y. Wang, S. Huang, Y.C. Zhao, Sci. Total Environ. **615**, 422 (2018)
31. Y. Xiang, X.D. Ru, J.G. Shi, J. Song, H.D. Zhao, Y.Q. Liu, D.D. Guo, X. Lu, J. Agric. Food Chem. **65**(50), 10851 (2017)
32. R. Liang, M. Liu, J. Agric. Food Chem. **54**, 1392 (2006)
33. S.Y. Lü, C. Feng, C.M. Gao, X.G. Wang, X.B. Xu, X. Bai, N.N. Gao, M.Z. Liu, J. Agric. Food Chem. **64**(24), 4965 (2016)
34. A. Rashidzadeh, A. Olad, D. Salari, A. Reyhanitabar, J. Polym. Res. **21**(2), 1 (2014)
35. E.-R. Kenawy, M.M. Azaam, E.M. El-nshar, Polym. Adv. Technol. **29**(7), 2072 (2018)
36. S. Li, X. Liu, Polym. Adv. Technol. **19**, 371 (2008)
37. A. Bajpai, J. Shrivastava, Polym. Int. **54**, 1524 (2005)

Publisher's Note Springer Nature remains neutral with regard to jurisdictional claims in published maps and institutional affiliations.